HIGH TEMPERATURE MATERIAL PROCESSES

An International Journal

Volume 9, Number 3, 2005

Jacques Amouroux
Pierre Fauchais
Editors

Numerical modeling for a better understanding of gas discharge plasmas

Annemie Bogaerts, Kathleen De Bleecker, Violeta Georgieva, Dieter Herrebout, Ivan Kolev, Myriam Madani and Erik Neyts
University of Antwerp, Department of Chemistry,
Universiteitsplein 1, B-2610 Wilrijk-Antwerp, Belgium.
E-mail: Annemie.Bogaerts@ua.ac.be

Abstract

We present here some of our modeling efforts for gas discharge plasmas, used in a number of applications in materials science. Different kinds of modeling approaches are applied, including fluid models, particle-in-cell – Monte Carlo (PIC-MC) models and hybrid Monte Carlo – fluid models, for the plasma behavior, as well as molecular dynamics simulations for thin film growth. The application fields include the deposition of amorphous hydrogenated carbon layers (diamond-like carbon) from hydrocarbon plasmas, the dust formation in silane discharges, the surface treatment with dielectric-barrier discharges, magnetron discharges used for sputter-deposition, dual-frequency capacitively coupled radio-frequency (cc-rf) discharges in $CF_4/Ar/N_2$, for etching applications, and glow discharges for spectrochemical analysis of materials.

Keywords: plasma, gas discharge, modeling, fluid model, PIC-MC model, hybrid model, molecular-dynamics simulations.

1. Introduction

Gas discharge plasmas are used in a range of applications fields, such as light sources, lasers, plasma display panels, in the semiconductor industry (for etching of surfaces and deposition of thin layers), in materials technology (for surface modification, deposition of protective coatings,…), in analytical chemistry (for the analysis of mainly solid materials), for biotechnological and environmental applications, etc. [1]. To make progress in these application fields, it is desirable to obtain a better insight in the plasma processes. We try to obtain this by numerical modeling.

There exist different kinds of modeling approaches to describe gas discharge plasmas. In ***analytical models*** [2,3] an analytical derivation of the plasma behavior is made, yielding

explicit formulas describing dependences of certain parameters from macroscopic quantities (such as voltage, current, pressure). This method is very fast, and can easily predict the plasma behavior, but it is only an approximation, valid for a limited range of conditions.

A ***fluid model*** [4,5] is based on the velocity moments of the Boltzmann transport equation (continuity equations of particle density, momentum density and energy density), usually coupled to Poisson's equation to calculate a self-consistent electric field distribution. It is in principle also quite simple and fast (although it can be tricky to solve the set of coupled differential equations), but it is only approximate, because it assumes that the plasma species are more or less in equilibrium with the electric field, which is not always true, e.g., for the fast electrons in regions characterized by a strong electric field, where they gain more energy from the electric field than they lose by collisions.

By solving the ***Boltzmann transport equation*** [6,7], the non-equilibrium behavior of the plasma species is fully accounted for. However, this approach can become mathematically very complicated.

Monte Carlo (MC) simulations [8,9], on the other hand, are mathematically simple, and they also account correctly for the non-equilibrium behavior of the plasma species. They describe the trajectories of individual particles by Newton's laws, and treat the collisions (occurrence of a collision, kind of collision, new energy and direction after collision) by random numbers. In order to reach statistically valid results, a large number of individual particles needs to be simulated. Hence, MC simulations are very time-consuming, especially for slow-moving particles. Moreover, a MC model on its own is not "self-consistent", because it requires a certain electric field distribution as input value.

This problem is overcome by the ***particle-in-cell – Monte Carlo (PIC-MC)*** method [10,11], which couples MC simulations for the behavior of ions and electrons, to the Poisson equation for a self-consistent electric field distribution. However, this makes this modeling approach even more time-consuming.

It is clear that every modeling approach has its own advantages and disadvantages, and will be most suitable for a specific kind of problem. For instance, a PIC-MC model is particularly interesting for very low pressure discharges, where the plasma species can have high energies and are not in equilibrium with the electric field. It is, however, not so suitable to describe the plasma chemistry in great detail, because it becomes too time-consuming for a large number of different plasma species. For the latter application, a fluid model is more

appropriate, because the computation time does not increase to the same extent as for a PIC-MC model, when describing more species and more chemical reactions.

Finally, ***hybrid models*** [12,13] are also interesting for some applications, because they are a combination of different models for the different species (e.g., MC models for fast plasma species, which are not in equilibrium with the electric field, and fluid models for slow species, which can be considered in thermal equilibrium). In this way, hybrid models can get rid of some of the disadvantages, and benefit from the advantages of the different models.

We have used several of these modeling approaches to describe the plasma processes for various applications. Moreover, we also try to simulate the plasma-wall interactions, for instance, the processes taking place in thin film deposition. For this purpose, we use ***molecular dynamics (MD) simulations*** [14], which treat the processes by Newton's laws, using the interaction potentials between all species. In the following, we will give a few examples of our modeling efforts for selected applications in materials science.

2. Fluid modeling

2.1. Capacitively coupled radio-frequency (cc-rf) discharge in hydrocarbon plasmas, used for diamond-like carbon deposition

Diamond-like carbon (DLC) layers can be deposited by cc rf discharges, operating both in methane (CH_4) [15] and in acetylene (C_2H_2) [16]. We have therefore developed a fluid model for cc rf discharges in CH_4 and in C_2H_2 plasmas, both in the pure feed gases as well as in mixtures with H_2, Ar or He [17,18]. It appears that both discharge gases give rise to a quite different plasma chemistry, so that different species (i.e., molecules, radicals, ions and electrons) had to be taken into account (see Tables 1 and 2).

In the CH_4 model, 27 electron-neutral reactions (vibrational excitation, dissociation, ionization), 7 ion-neutral and 12 neutral-neutral chemical reactions were taken into account, whereas the C_2H_2 model considered 19 electron-neutral reactions, 1 ion-neutral and 17 neutral-neutral reactions. The reaction rate coefficients of the ion-neutral and neutral-neutral reactions are taken from literature. The rate coefficients of the electron-neutral reactions depend strongly on the average electron energy, and are, therefore, obtained from a simplified Boltzmann equation (see refs. [17,18] for more details).

Table 1: Different species taken into account in the CH_4 plasma model:

Molecules		Radicals		Ions			Electrons
CH_4	H_2	C_2H_5	CH_3	CH_3^+	CH_4^+	CH_5^+	e^-
C_2H_6	C_3H_8	CH	CH_2	$C_2H_5^+$	$C_2H_4^+$	$C_2H_2^+$	
C_2H_4	C_2H_2	H		H_3^+	H_2^+		

Table 2: Different species taken into account in the C_2H_2 plasma model:

Molecules	Radicals				Ions		Electrons
C_2H_2	C_2H	C_4H	C_6H	C_8H	$C_2H_2^+$	C_2H^+	e^-
H_2	C_4H_2	C_6H_2	C_8H_2		C_2^+	CH^+	
	C_2H_3	C_4H_3	C_6H_3		C^+	H_2^+	
	CH	CH_2	H		$C_4H_2^+$	$C_6H_2^+$	

For every plasma species, a continuity and transport equation are constructed. The continuity equations are balance equations, taking into account all different production and loss mechanisms for the species:

$$\frac{\partial n_k}{\partial t} + \overline{\nabla}.\overline{\Gamma}_k = S_{prod,k} - S_{loss,k}$$

n_k and $\overline{\Gamma}_k$ represent the density and flux of species k, and $S_{prod,k}$ and $S_{loss,k}$ describe the rate of production and loss of species k, respectively.

The transport equation is based on diffusion for the neutral particles (molecules, radicals) and on diffusion and migration under influence of the electric field for the charged particles (ions, electrons):

$\overline{\Gamma}_e = -\mu_e n_e \overline{E} - D_e \overline{\nabla} n_e$ for the electrons

$\overline{\Gamma}_i = \mu_i n_i \overline{E} - D_i \overline{\nabla} n_i$ for the ions

$\overline{\Gamma}_n = -D_n \overline{\nabla} n_n$ for the neutrals

μ and D are the mobility and diffusion coefficients, respectively.

An energy balance equation is also incorporated for the electrons:

$$\frac{\partial n_e \varepsilon}{\partial t} + \overline{\nabla} \cdot \overline{\Gamma}_w = -e\overline{\Gamma}_e \cdot \overline{E} + S_w$$

ε is the average electron energy. The first term on the right-hand side gives the Ohmic heating and the second term (S_w) describes the loss of energy due to electron impact collisions. $\overline{\Gamma}_w$ is the energy flux and can again be described by a drift-diffusion approximation:

$$\overline{\Gamma}_w = \frac{5}{3}\mu_e n_e \varepsilon \overline{E} - \frac{5}{3} D_e \overline{\nabla} n_e \varepsilon$$

The other plasma species are assumed to be in thermal equilibrium, so that no energy balance equation has to be considered. Finally, all these equations are coupled to Poisson's equation to obtain a self-consistent potential distribution:

$$\Delta V = -\frac{e}{\varepsilon_0}(n_i - n_e)$$

This system of non-linear coupled differential equations is solved numerically with the Scharfetter-Gummel exponential scheme.

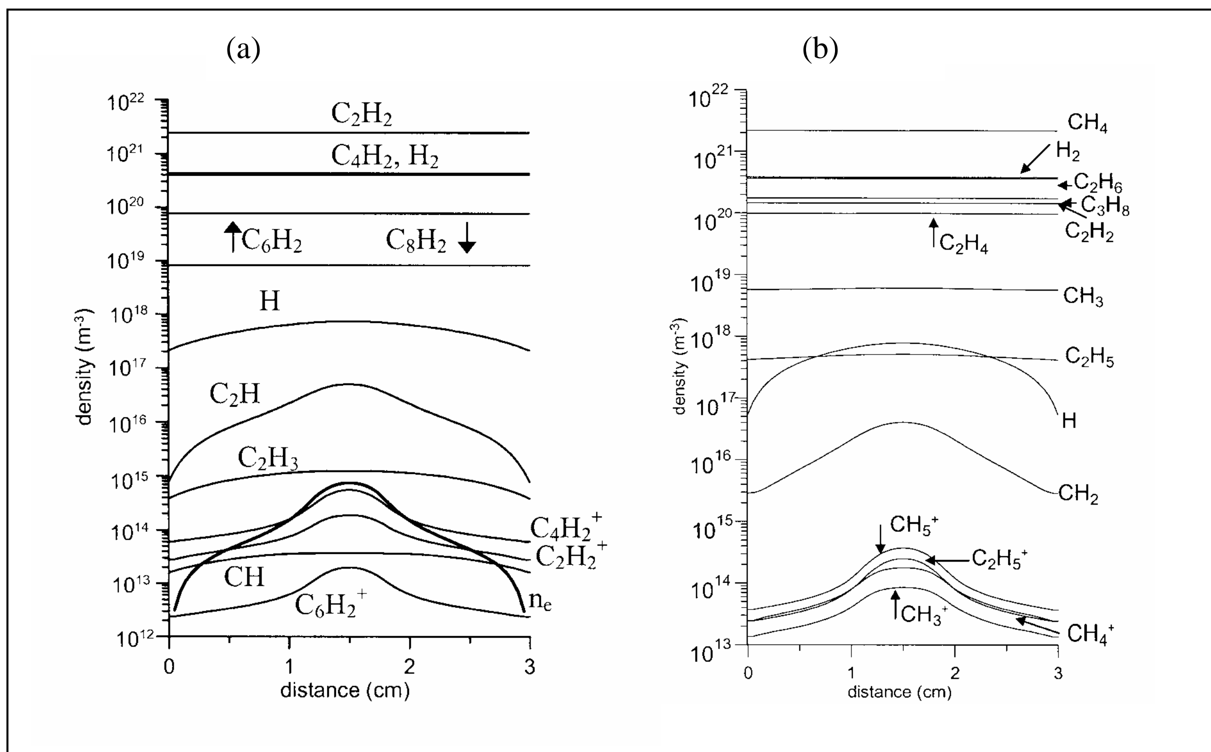

Figure 1: Calculated time-averaged density profiles of the most important plasma species, for a cc rf discharge in CH_4 (a) and in C_2H_2 (b), at a gas pressure of 0.14 Torr, an electrical power of 10 W, and an input gas flow of 20 sccm CH_4 or C_2H_2, respectively. Reproduced from [17,18] with permission of American Institute of Physics and IEEE, respectively.

Figure 1 shows the calculated density profiles of the most important molecules, radicals and ions, as well as the electrons, as a function of distance between the electrodes, for the CH_4 discharge (a) and the C_2H_2 discharge (b), at a gas pressure of 0.14 Torr, an electrical power of 10 W, and an input gas flow of 20 sccm CH_4 or C_2H_2, respectively. It is indeed clear from these figures that both gases yield a completely different plasma chemistry. In the acetylene discharge, mainly higher order radicals (C_4H_2, C_6H_2, C_8H_2) are formed at high densities, whereas in the methane plasma, the molecules C_2H_2, C_2H_4, C_2H_6 and C_3H_8 are abundant at relatively high densities, and the most important radicals are CH_3, H and C_2H_5. The fact that other radicals and molecules are present at high densities in both plasmas is attributed to the different neutral-neutral chemistry in both plasmas [17,18].

2.2. Dust formation in a silane cc-rf discharge

The formation of dust (i.e., particles with dimensions in the nm to μm range) in plasma discharges is a topic of growing interest. Initially, these nanoparticles were considered to be harmful, because they contaminated the substrate (for deposition or etching applications). Moreover, in the micro-electronics industry, particles with dimensions in the (sub-)μm range can cause killer defects [19]. Therefore, initially, the international research aimed at avoiding the particle formation. However, in recent years, it has become clear that nano-particles in plasmas can lead to very interesting applications. For instance, film deposition in solar cell applications seems to benefit from the presence of nanoparticles, because the latter can be incorporated in the deposited films [20]. The so-called polymorphous silicon thin films have superior electric properties, making this material a good candidate for use in high-efficiency solar cells [19].

To better understand the mechanisms responsible for nanoparticle growth in the plasma, and to be able to predict at which conditions these nanoparticles can be incorporated in the deposited layer, we are developing a fluid model for a cc rf discharge operating in silane [21,22]. This model is based on the fluid model developed earlier by Nienhuis and Goedheer for a cc rf discharge in silane without dust formation [23], but a large number of plasma species and reactions are added, based on the model by Bhandarkar [24]. The model now considers 68 species, including molecules, radicals, (positive and negative) ions and electrons (see Table 3).

Table 3: Overview of the different species incorporated in the dusty plasma chemistry model for the SiH_4 cc rf discharge , beside the electrons.

Molecules	Ions	Radicals
SiH_4, $SiH_4^{(2-4)}$, $SiH_4^{(1-3)}$	SiH_3^+, $Si_2H_4^+$	SiH_3, SiH_2
H_2	H_2^+	H
	SiH_3^-, SiH_2^-	
Si_2H_6, Si_3H_8, Si_4H_{10}, Si_5H_{12}	$Si_2H_5^-$, $Si_3H_7^-$, $Si_4H_9^-$, $Si_5H_{11}^-$	Si_2H_5,Si_3H_7, Si_4H_9, Si_5H_{11}
Si_6H_{14}, Si_7H_{16}, Si_8H_{18}, Si_9H_{20}	$Si_6H_{13}^-$, $Si_7H_{15}^-$, $Si_8H_{17}^-$, $Si_9H_{19}^-$	Si_6H_{13}, Si_7H_{15}, Si_8H_{17}, Si_9H_{19}
$Si_{10}H_{22}$, $Si_{11}H_{24}$, $Si_{12}H_{26}$	$Si_{10}H_{21}^-$, $Si_{11}H_{23}^-$, $Si_{12}H_{25}^-$	$Si_{10}H_{21}$, $Si_{11}H_{23}$, $Si_{12}H_{25}$
	$Si_2H_4^-$, $Si_3H_6^-$, $Si_4H_8^-$, $Si_5H_{10}^-$	Si_2H_4, Si_3H_6, Si_4H_8, Si_5H_{10}
	$Si_6H_{12}^-$, $Si_7H_{14}^-$, $Si_8H_{16}^-$, $Si_9H_{18}^-$	Si_6H_{12}, S_7H_{14}, Si_8H_{16}, Si_9H_{18}
	$Si_{10}H_{20}^-$, $Si_{11}H_{22}^-$, $Si_{12}H_{24}^-$	$Si_{10}H_{20}$, $Si_{11}H_{22}$, $Si_{12}H_{24}$

In addition to SiH_4 ground state molecules, vibrationally excited SiH_4 molecules, formed by electron impact collisions on ground state SiH_4, i.e., $SiH_4^{(2-4)}$ at 0.113 eV, and $SiH_3^{(1-3)}$, at 0.271 eV, are also considered. Silicon hydrides (Si_nH_m) up to a maximum of 12 Si-atoms are taken into account. For every saturated silicon hydride molecule Si_nH_{2n+2}, the corresponding Si_nH_{2n+1} radical has to be considered, since H-abstraction is an important reaction in silane plasmas. The silylenes Si_nH_{2n} are also included, since their corresponding anions play a role in the initial particle formation. The silylenes are a reactive form of the silenes (i.e., molecules containing a double bond between two silicon atoms), and they are characterized by a single bond between the two silicon atoms with two non-bonding electrons. While the positive ions are limited to SiH_3^+, $Si_2H_4^+$ and H_2^+, the negative ions are extended up to species containing 12 Si-atoms, because they determine the reaction pathway of nanoparticle growth [24]. We make a distinction between the silyl anions ($Si_nH_{2n+1}^-$) and the silylene anions ($Si_nH_{2n}^-$), because they correspond to the different sets of radicals.

Figure 2 shows the calculated density profiles of the various molecules, radicals, positive and negative ions, for a cc rf discharge, at a pressure of 40 Pa and a power of 5 W. It is clear that the molecules are uniformly distributed in the plasma (figure 2a), whereas the excited molecules, the radicals, ions and electrons go to low values at the reactor walls (figures 2a, b, c, d). Further, it is found that the anion SiH_3^- is the most important primary

precursor of the particle formation. Over 90% of the nano-particle formation proceeds through the silyl anion ($Si_nH_{2n+1}^-$) pathway, starting from SiH_3^-, and only about 10% goes through the silylene anion ($Si_nH_{2n}^-$) pathway, starting from SiH_2^-. More details about this model (e.g.,

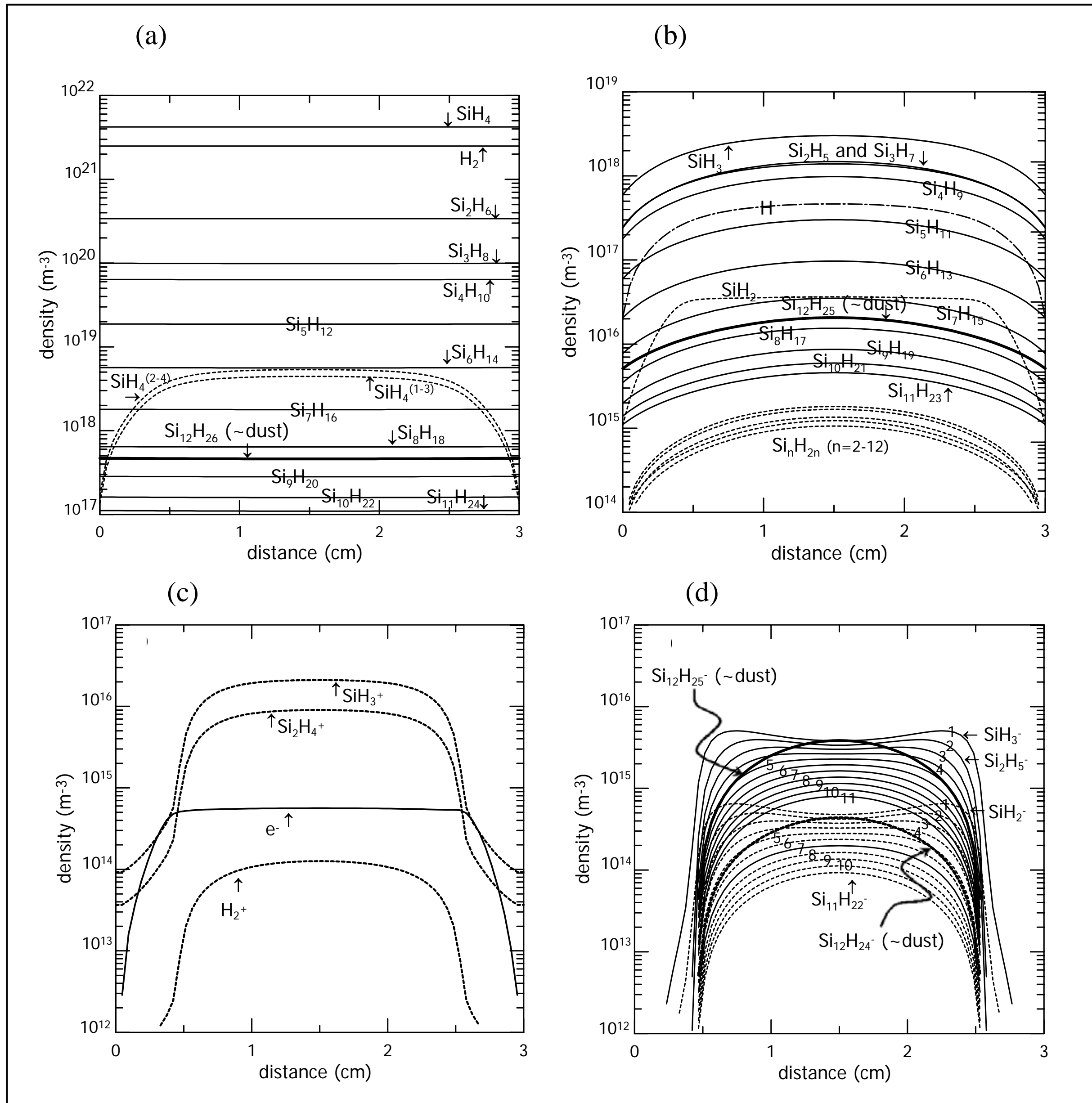

importance of various chemical reaction mechanisms, etc) can be found in [22].

<u>Figure 2:</u> Calculated time-averaged density profiles of the Si_nH_{2n+2} molecules and the vibrationally excited SiH_4 molecules (a), the silyl radicals (Si_nH_{2n+1}) and the silylenes (Si_nH_{2n}) (b), the positive ions and electrons (c), and the various negative ions (d), for a cc rf discharge in SiH_4, at a pressure of 40 Pa and a power of 5 W. The numbers labelling the curves in

figure 2d correspond to the number of Si-atoms in the anions. Reproduced from [22] with permission of the American Physical Society.

As shown in Table 3 and figure 2, this model describes the detailed plasma chemistry and cluster growth for silicon-hydrides up to 12 Si-atoms. However, in a real silane cc rf discharge, the dust formation goes on to larger particles (with dimensions in the nm, and even μm range). It is, however, not possible to describe the detailed plasma chemistry for an unlimited number of plasma species. Therefore, the detailed plasma chemistry model stops at species with 12 Si-atoms, and the further growth is calculated with a coagulation model, like described in [25]. Also the charging of the dust particles [26], and their transport (as a result of different forces: electrostatic, gravity, ion drag, neutral drag and thermoforetic force) [27] is described. A paper about this work is in preparation [28].

2.3. Atmospheric pressure dielectric barrier discharge

As mentioned in the introduction, fluid modeling is especially useful when the detailed plasma chemistry has to be simulated, like in the examples shown above, and also when the discharge pressure is sufficiently high, so that the plasma species undergo many collisions, and can be considered more or less in equilibrium with the electric field. In this respect, fluid models are the logical choice for gas discharges at atmospheric pressure, such as dielectric barrier discharges (DBDs).

We have recently developed a fluid model for a DBD in N_2, at 1 atm [29], used for materials science applications, such as deposition and activation of layers [30]. The species taken into account in this model, are: N_2 molecules, N atoms, N_2 molecules in excited states (in the $A\,^3\Sigma_u^+$ and $a'\,^1\Sigma_u^-$ levels), N^+, N_2^+, N_3^+ and N_4^+ ions. The vibrational chemistry of N_2 was not yet included.

Beside the continuity and transport equations for every species, the electron energy balance equation and the Poisson equation, which are common for all fluid models described in this paper, there are some additional equations in the fluid model for the DBD. Indeed, the DBD consists of two parallel electrodes, and one or both electrodes is covered with an insulating material (glass, alumina,…). Hence, the presence of this dielectric needs to be taken into account by means of the appropriate boundary conditions for the potential. Also secondary electron emission and electron desorption from the dielectric, when the polarity of the electric field is switched, have to be taken into account, by adding two extra terms for the

electron flux at the boundary. This yields a modified boundary condition for the electron density, compared to a fluid model for a plasma discharge between two conducting electrodes. More details can be found in ref. [29].

A DBD at atmospheric pressure can give rise to a uniform or to a filamentary discharge, and the uniform DBD can be either in glow mode or Townsend mode, depending on the width of the discharge gap, the kind of dielectric and its thickness [31]. In a Townsend discharge, the electron density rises from the instantaneous cathode to the instantaneous anode, and the ion density exceeds the electron density by several orders of magnitude, so that there is no charge-neutrality in the plasma [31]. In the glow mode, on the other hand, the bulk of the discharge is quasi-neutral, like in a low-pressure glow discharge. Hence, the density profiles calculated with our model can give us an indication about which kind of discharge mode will be obtained for a certain parameter set.

Figure 3 shows the calculated 2D density profiles of the electrons and of the sum of all positive ions, at $\omega t = \pi/2$, for a DBD with a gap of 1 mm, operating at a frequency of 10 kHz and 10 kV voltage amplitude. It is clear that the discharge is fairly uniform in the radial direction, which is good for surface engineering applications.. Moreover, the total positive ion density exceeds the electron density by several orders of magnitude, and the electron density rises from the instantaneous cathode towards the instantaneous anode. Hence, we can conclude that for the operating conditions shown in this figure, the DBD is uniform and in the Townsend mode. This is in agreement with literature [32]. We are currently performing a detailed parameter study with our 2D model, to investigate the influence of frequency, applied power and geometry on the structure of the DBD (i.e., uniform vs. filamentary, Townsend vs. glow mode).

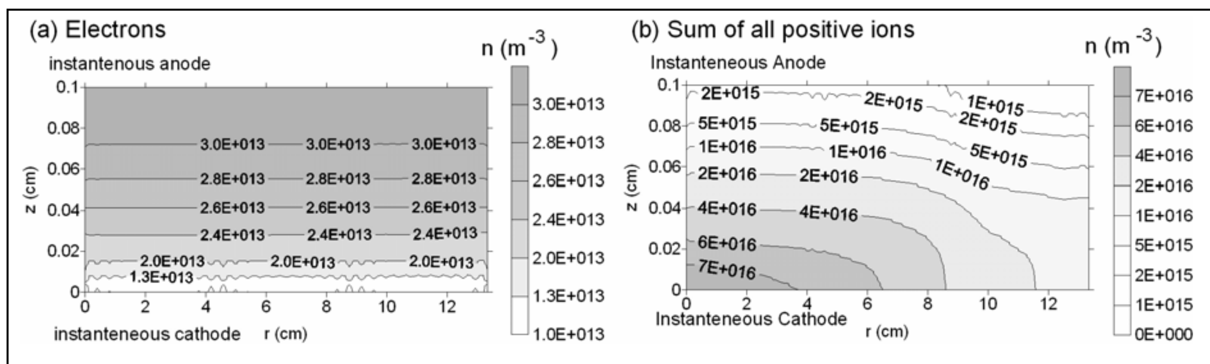

Figure 3: Calculated 2D density profiles of the electrons (a) and the sum of all positive ions (b), throughout the discharge, at $\omega t = \pi/2$, for a DBD in N_2, with a gap of 1 mm, operating at a frequency of 10 kHz and 10 kV voltage amplitude.

3. PIC-MC modeling

3.1. Dual frequency cc-rf discharge in $Ar/SiF_4/N_2$

Fluid modeling is very useful for describing the detailed plasma chemistry, but for some applications (e.g., plasma etching), other information is required, such as the energy distributions of the species bombarding the target, because this determines for instance the etching rate. This information cannot be obtained with fluid models. In PIC-MC simulations, on the other hand, this information is readily available, since the behavior of individual plasma particles is simulated, including the details of energy gain from the electric field, and the energy losses through collisions [33]. A PIC-MC model is particularly useful for treating charged particles (ions and electrons). These particles are replaced by superparticles, with a weight (i.e., number of real particles per superparticle) in the order of 10^7-10^9 (depending on the ion and electron densities). During successive time-steps, the movement of the superparticles under the influence of the electric field is simulated with Newton's laws. After each time-step, the charge density is calculated from the particles coordinates and assigned to the computational grid nodes, on which subsequently the Poisson equation is solved. This yields a new electric field on each grid node, which is linearly interpolated to each particle position. After that, the particles are moved again during the next time-step. The collisions (i.e., occurrence of a collision during each time-step, kind of collision and new energy and direction after collision) are treated with random numbers, in the Monte Carlo part of the model.

The PIC-MC model that we have developed for a cc rf discharge in a mixture of $CF_4/N_2/Ar$, typically used for plasma etching of silicon and silicon dioxide in the semiconductor industry [34], considers the following species: electrons, Ar^+, CF_3^+, N_2^+, F^- and CF_3^- ions. 41 different electron-neutral collisions, 2 electron-ion recombination reactions, 4 positive – negative ion recombination reactions and about 130 ion-neutral chemical reactions, are taken into account in the model (see refs [35,36] for more details).

Since Ar is a typical electropositive gas, and CF_4 is an electronegative gas, a study of different Ar/CF_4 gas mixtures can give us a better insight in the different behavior of electropositive and electronegative gas discharges. Figure 4 shows the calculated density

profiles of the various ions and the electrons, in the cc rf discharge, for three different ratios of Ar/CF_4 (without N_2), for a total gas pressure of 200 mTorr and a voltage amplitude of 200 V [35]. At high Ar concentration (90%; figure 4a), the discharge shows the characteristics of an electropositive discharge, but some aspects of electronegative discharges begin to appear already. Indeed, the dominant negative species are not the electrons, but the negative ions (mainly F^-). Also, the electron density is quite flat in the bulk plasma, instead of showing a maximum in the center. The major positive ions are Ar^+, and the density of CF_3^+ ions is about two orders of magnitude lower than that of Ar^+. At equal concentrations of Ar and CF_4 (figure 4b), the discharge exhibits more electronegative features. The electron density has dropped further, and the negative ion densities become higher. Also, the electron density profile is not completely flat anymore, but small peaks are formed at the bulk-sheath interface. The Ar^+ ion is still the major positive ion, because of the larger ionization cross section of argon compared to that of CF_4. However, the density of CF_3^+ ions is now only less than a factor of 4 lower than the Ar^+ ion density. At high concentration of CF_4 (90%, figure 4c), the discharge structure is definitely electronegative. The electron density has dropped further, and the maxima at the bulk-sheath interface are more pronounced. The major positive ion is now

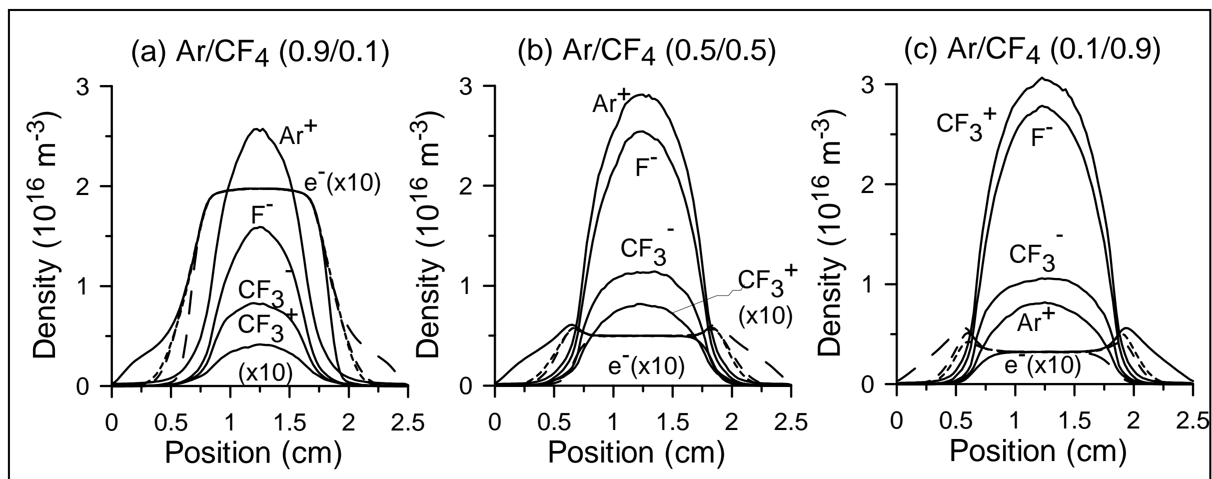

CF_3^+. More information about this calculated behavior of the Ar/CF_4 discharge in different gas ratios, and the transition between electropositive and electronegative discharges, can be found in [35].

Figure 4: Calculated density profiles of the various ions (time-averaged) and the electrons (at different times), in a cc rf discharge, in a mixture Ar/CF_4, in different ratios: (a) 0.9/0.1, (b)

0.5/0.5, (c) 0.1/0.9, at a total gas pressure of 200 mTorr, a voltage amplitude of 200 V, and frequency of 13.56 MHz.

In recent years, there is a growing interest in dual frequency cc rf discharges for plasma etching applications, i.e., using two frequencies instead of one (e.g., [37]). Indeed, dual frequency systems allow the precise and independent control of both ion bombardment energy and ion flux. The plasma density is determined by the source of high frequency (e.g., 13.56 or 27 MHz) or very-high frequency (100 MHz), while the substrate self-bias voltage is controlled by the low frequency (e.g., order of 1-2 MHz). In addition, a dual frequency setup provides a wider ion bombardment energy in comparison with a single frequency scheme. Therefore, we have studied in detail the behavior of dual-frequency cc rf discharges in a mixture $Ar/CF_4/N_2$, and comparison is made with single-frequency reactors [36,38]. Figure 5 illustrates calculated ion energy distribution functions (IEDFs) at the powered electrode, for Ar^+, CF_3^+ and N_2^+ ions, averaged over one rf-cycle in the single-frequency (13.56 MHz) cc rf reactor (a and b), and averaged over two low-frequency cycles in the dual-frequency (2 + 27 MHz) reactor (c and d). The reason that averaging is performed over two low-frequency cycles is because one low-frequency cycle does not contain an integer number of high-frequency cycles [36].

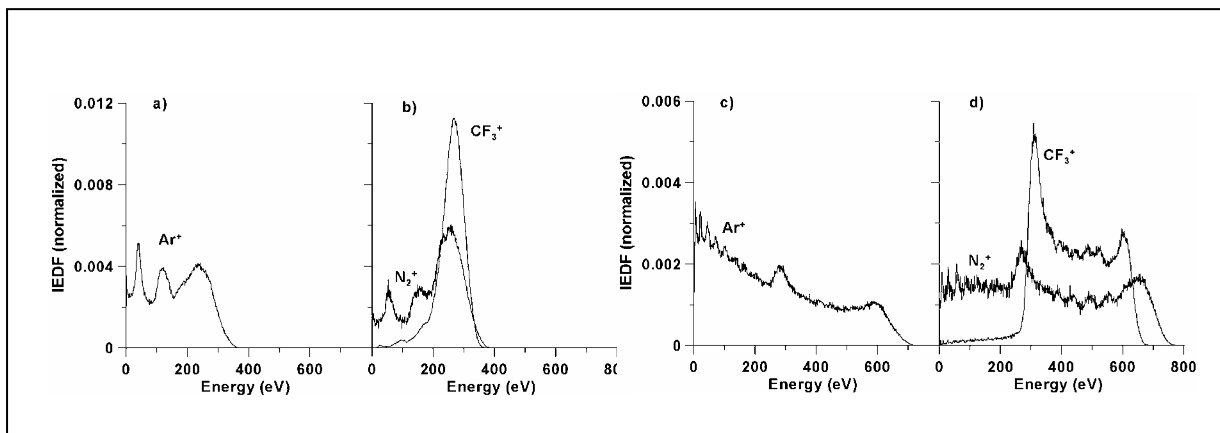

Figure 5: Calculated time-averaged ion energy distribution functions (IEDFs) at the powered electrode, for Ar^+, CF_3^+ and N_2^+ ions, in a single-frequency (13.56 MHz) cc rf reactor (a and b), and in a dual-frequency (2 + 27 MHz) reactor (c and d), for a pressure of 30 mTorr and

applied voltage amplitude of 700 V. Reproduced from [36] with permission of American Institute of Physics.

It is indeed clear that the IEDFs in the single-frequency reactor are quite narrow, with typically one outstanding peak, and possibly secondary peaks at lower energy, because of energy losses through collisions. The IEDFs in the dual-frequency reactor, on the other hand, are broad and bimodal, and the two outstanding peaks in the profiles correspond to the averaged minimum and maximum sheath potential drop [36,38]. Further, the IEDF width depends on the ion mass, i.e., a lower mass yields a broader IEDF (cf. figure 5d). More information about this study of single and dual frequency cc rf reactors can be found in refs. [36,38].

3.2. Magnetron discharge

Another application area for which we use PIC-MC simulations, are the magnetron discharges, commonly used for sputter-deposition of thin films. In a magnetron discharge, a magnetic field is applied to the discharge plasma, beside the electric field (potential difference between the electrodes). Because the electrons are trapped in the magnetic field, their path length and residence time in the plasma is significantly increased, so that they give rise to more ionization collisions, and hence more electron multiplication, than in a discharge plasma without magnetic field. Hence, magnetron discharges can operate at much lower pressure, for the same electric power as in a normal gas discharge. Because of this low pressure, and because the electron movement needs to be followed on a microscopic scale, in order to capture the correct physics, PIC-MC simulation are the best choice [39].

Figure 6 shows a typical dc planar magnetron discharge geometry. The magnet is placed behind the target, and the magnetic field strengths are indicated with the arrows. The maximum magnetic field strength is found in front of the target, at about 1.8 cm from the cylinder axis (cfr. largest arrows in the figure). Figure 7 illustrates the calculated potential distribution (a) and electron impact ionization rate (b), for the magnetron shown in figure 6. It is clear from figure 7a that the cathode dark space is shortest, and hence the electric field is strongest, at about 1.8 cm from the cylinder axis, i.e., where the magnetic field strength is at maximum. Also the electron impact ionization rate is highest in this region (see figure 7b), because (i) the electrons gain most energy from the electric field, and (ii) they are trapped in

the magnetic field lines. Consequently, also the charged particle (ion and electron) densities are highest in this region.

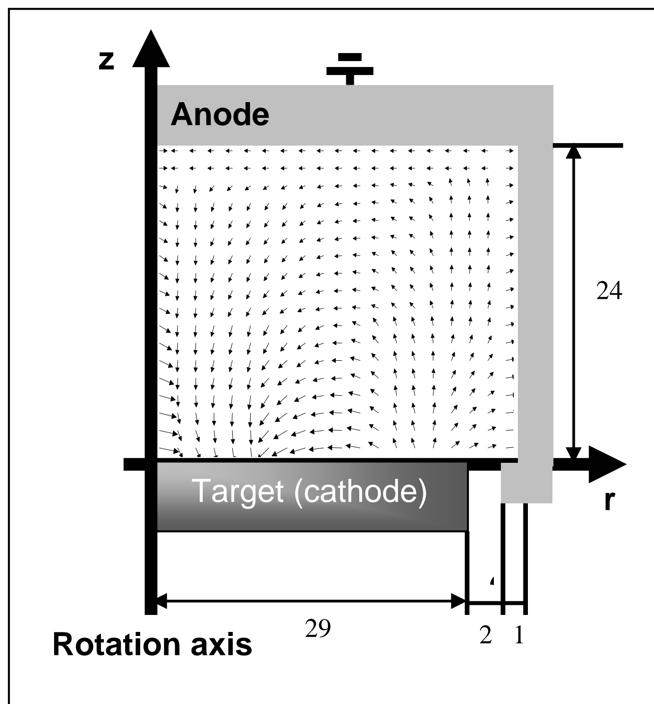

Figure 6: Magnetron discharge geometry and dimensions, as well as magnetic field lines, used for the calculations. The maximum magnetic field strength, indicated by the longest arrows (i.e., in front of the target, at about 1.8 cm from the cylinder axis), is 300 G. The dimensions are indicated in mm.

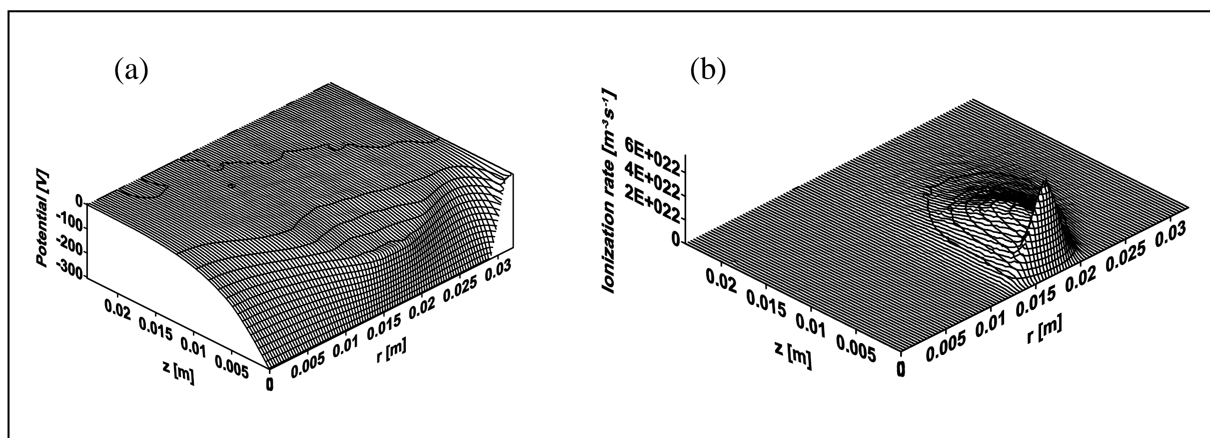

<u>Figure 7:</u> Calculated potential distribution (a) and electron impact ionization rate (b) in the magnetron discharge shown in figure 6, at an argon gas pressure of 4.2 mtorr, a voltage of 350 V, and an electrical current of 250 mA.

4. Hybrid MC – fluid modeling

As mentioned in the introduction, an alternative to PIC-MC simulations is given by the hybrid MC – fluid model, where the energetic plasma species are simulated with MC models, and the slow plasma species are treated with the fluid approach. Such a hybrid model should not be limited to two models, but it can combine several models to describe the various species present in the plasma.

A "hybrid modeling network" was developed in our group for a glow discharge used for spectrochemical analysis of (mainly solid) materials (e.g., [40]). In this application, the material to be analyzed is used as the cathode of the glow discharge, and it is sputtered by the bombardment of energetic plasma species. The sputtered, analytically important, atoms arrive in the glow discharge plasma, where they are subject to ionization and excitation collisions, yielding ions and/or excited atoms of the material to be analyzed. The ions can be measured in a mass spectrometer, whereas the excited atoms emit characteristic photons which can be detected with optical emission spectrometry. Hence, for this application, not only the discharge gas species (e.g., argon) are important, but special interest goes to the sputtered species. Moreover, because the glow discharge is often used in combination with optical emission spectrometry, the behavior of atoms in various excited levels is also of interest. The latter species are typically treated with collisional-radiative models, which is a kind of fluid model, i.e., it consists of a set of balance equations (one for each level) with different production and loss terms. The species taken into account in this hybrid modeling network, as well as the models used to describe their behavior, are presented in Table 4.

Due to the interaction processes between the species, the various models are coupled to each other, i.e., the output of one model is used as input in the next model. For instance, the MC models calculate the rates of the various collisions (electron, fast argon ion or atom impact ionization and excitation), which are used as input in the fluid and collisional-radiative models (production and loss terms for the various species). Vice versa, the electric field

distribution, calculated by Poisson equation in the fluid model for Ar^+ ions and electrons, is used as input in the Monte Carlo models. More information about this model can be found e.g. in [40].

With this hybrid modeling network, a lot of information can be obtained about different plasma quantities, such as the densities, fluxes and energies of the various plasma species, the electric field and potential distribution throughout the plasma, the importance of the various collision processes in the plasma, and of the various production and loss mechanisms for the different species, the sputtering (erosion) rate at the cathode, optical emission intensites, etc.

Table 4: Species taken into account in the hybrid modeling network for the spectrochemical glow discharge, as well as the models used to describe their behavior:

Plasma species	Model
Ar gas atoms	No model: assumed uniform + thermal
	Gas heating: heat transfer model
	Gas flow: computational fluid dynamics code
Energetic electrons	Monte Carlo model
Slow electrons	Fluid model
Ar^+ ions	Fluid model
Fast Ar^+ ions in cathode dark space (CDS)	Monte Carlo model
Fast Ar atoms in CDS	Monte Carlo model
Ar atoms in (64) excited levels	Collisional-radiative model
Sputtered atoms (e.g., Cu): thermalization	Monte Carlo model
Cu atoms in ground state + excited levels	Collisional-radiative model
Cu^+ ions in ground state + excited levels	Collisional-radiative model
Fast Cu^+ ions in CDS	Monte Carlo model

Of particular interest for the application of spectrochemical analysis of solid materials, are the crater profiles at the cathode, as a result of sputtering. Indeed, this technique is very often used for materials depth profiling, i.e., measuring the concentration of impurities as a function of depth in the solid material. It is clear that for this purpose, the crater profile should be as flat as possible, in order to sample the material from the same depth at the same time.

However, flat crater profiles are not always reached. Figure 8 shows calculated (a, b) and measured (c, d) crater profiles after glow discharge sputtering, for two different cell geometries, i.e., a Grimm-type source [41] which is designed to be very suitable for depth profiling (a, c) and an ion source for the VG9000 glow discharge mass spectrometer [42], which is not specifically designed for depth profiling (b, d). It is clear that the crater profiles obtained with the Grimm-type source are much more suitable for depth profiling than the

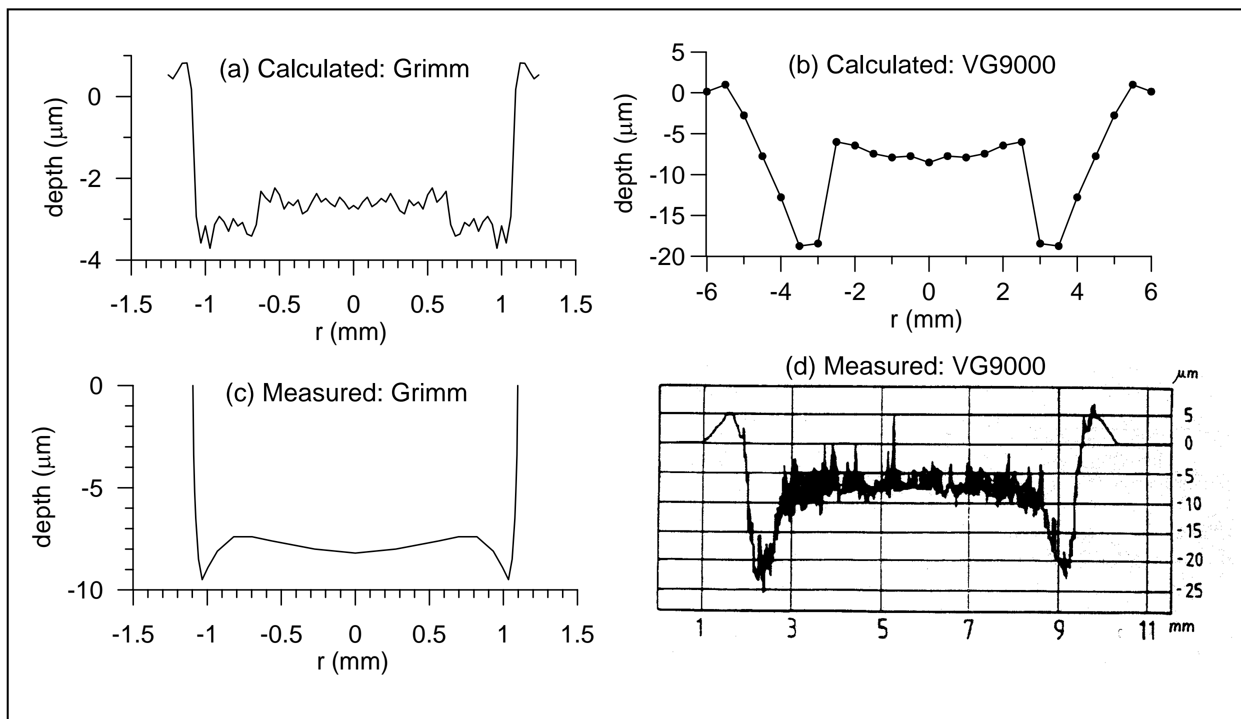

crater profiles obtained with the other source, which are much deeper at the sides than in the center. It also appears from this figure that the model calculations can back up the experimental results fairly well. Consequently, the model can be used to explain the specific crater shape, for certain conditions and cell design [41,42], and it can predict under which conditions optimal craters can be obtained.

Figure 8: Calculated (a, b) and measured (c, d) crater profiles after glow discharge sputtering, for a Grimm-type source (a, c) at a voltage of 880 V and a current of 5 mA, and for an ion source for the VG9000 glow discharge mass spectrometer (b,d) at a voltage of 1000 V and a current of 3 mA.

5. MD simulations

Finally, as mentioned in the introduction, beside modeling of the plasma processes, simulating the plasma-wall interactions is equally important for most applications in materials science. This can be done by MD simulations, which describe the behavior of the plasma species arriving at the substrate, by means of interatomic interaction potentials. We use an MD model, originally developed by Abrams [43], to simulate the plasma deposition of DLC layers, by means of the Brenner potential for hydrocarbons [44].

We have applied the MD model to some typical experimental conditions for the deposition of DLC layers in an expanding thermal Ar/C_2H_2 plasma [45]. The input in the model, i.e., the fluxes and energies of the species bombarding the substrate, are taken from experiment. Typical results of the model include the DLC film structure and composition, more specifically, the bonding network, the film density, the H-content, and the coordination number of C-atoms.

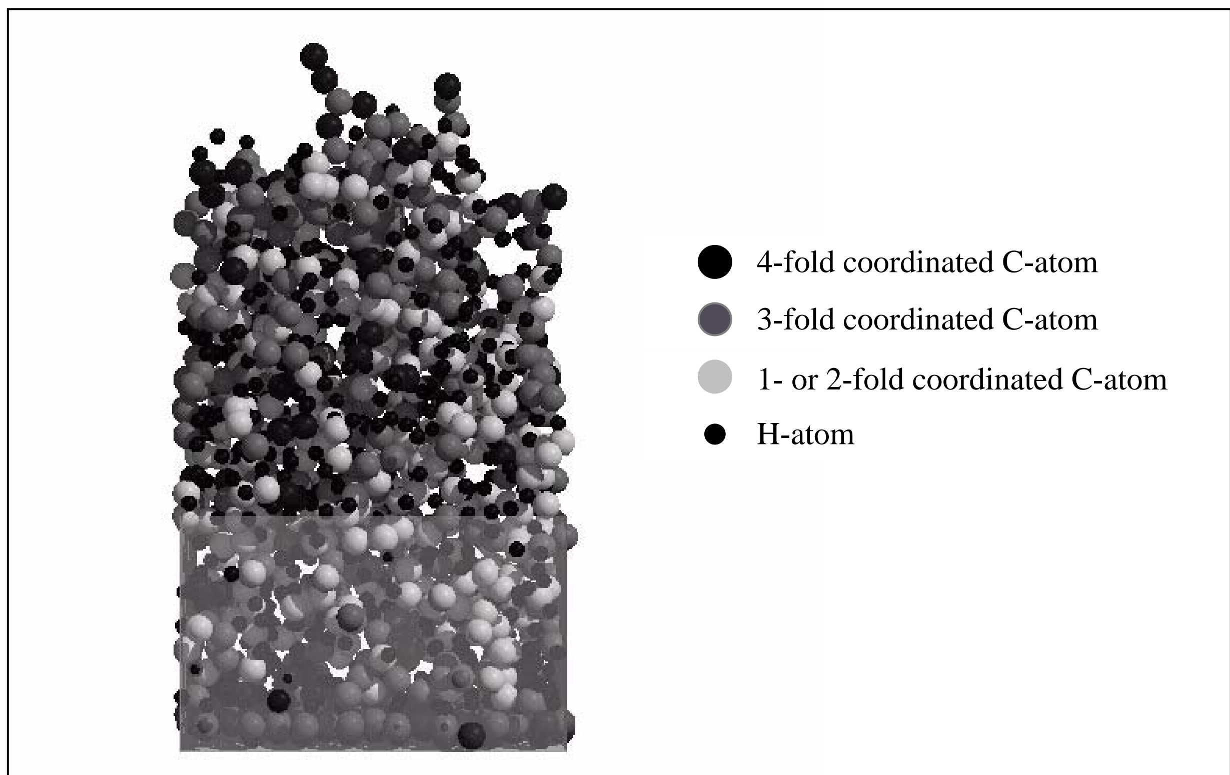

Figure 9: Simulated microscopic picture of a DLC film deposited from an expanding thermal Ar/C_2H_2 plasma.

Figure 9 shows the simulated microscopic picture of a film deposited when only C, C_2 and CH were identified (by the experimental measurements) as growth species, as well as a

large flux of H atoms. These conditions were obtained for an acetylene flux of $4.4\text{x}10^{21}$ m^{-2} s^{-1} (see ref. [46] for more details). The film deposited under these conditions was also measured with ELNES [47], and comparison was made between experimental and calculated results [46]. The fraction of 4-coordinated C-atoms, which is a measure for the fraction of sp^3 C-atoms, was calculated to be 0.50. This corresponds reasonably with the sp^3 fraction measured with ELNES (i.e., 0.67) [47]. Also the calculated H-concentration (i.e., 0.46) was in fair agreement with the experimental value (i.e., >0.42) [46]. This satisfactory agreement demonstrates that the MD simulations present a reasonably realistic picture of the deposited DLC films, and that they can therefore be used to obtain more insight in the deposition mechanism (i.e., relative importance of different species in the film growth, probability of etching the deposited film, etc).

6. Conclusion

In this paper, a few examples are presented of modeling efforts for a better understanding of the plasma processes, and plasma-wall interactions, in gas discharge plasmas, for various applications in materials science. Depending on the kind of problem (and discharge operating conditions), either fluid modeling, PIC-MC simulations or hybrid models are employed for the plasma behavior, whereas for the description of plasma-wall interactions, more specifically the deposition of DLC layers, MD simulations are carried out.

The examples show what kind of information can be expected from numerical modeling. In general, a better insight in the plasma behavior is acquired, which will be helpful for making progress in the application fields.

Acknowledgments

A. Bogaerts, V. Georgieva and I. Kolev are indebted to the Flemish Fund for Scientific Research (FWO) for financial support. K. De Bleecker and E. Neyts acknowledge financial support from the Institute for the Promotion of Innovation by Science and Technology in Flanders (IWT). Myriam Madani is supported from the Flemish Institute for Technological Research (VITO). The research is also sponsored by the IAP-V program.

References

1. A. Bogaerts, E. Neyts, R. Gijbels and J. van der Mullen, Gas discharge plasmas and their applications, Spectrochim. Acta Part B, 57 (2002) 609.
2. S. V. Berezhnoi, I. D. Kaganovich, L. D. Tsendin and V. A. Schweigert, Fast modeling of the low-pressure capacitively coupled rf discharge based on the nonlocal approach, Appl. Phys. Lett., 69 (1996) 2341.
3. Y. T. Lee, M. A. Lieberman, A. J. Lichtenberg, F. Bose, H. Baltes, and R. Patrick, Global model for high pressure electronegative radio-frequency discharges, J. Vac. Sci. Technol., 15 (1997) 113.
4. J.-P. Boeuf, Numerical model of rf glow discharges, Phys. Rev. A, 36 (1987) 2782.
5. J. D. P. Passchier and W. J. Goedheer, Relaxation phenomena after laser-induced photodetachment in electronegative rf discharges, J. Appl. Phys., 73 (1993) 1073.
6. I. Abril, Alacant: modeling of glow discharge sputtering systems, Comput. Phys. Commun. 51 (1988) 413.
7. R. J. Carman, A simulation of electron motion in the cathode sheath region of a glow discharge in argon, J. Phys. D, 22 (1988) 55.
8. M. J. Kushner, Mechanism for power deposition in Ar/SiH_4 capacitively coupled rf discharges, IEEE Trans. Plasma Sci., 14 (1986) 188.
9. Z. Donko, K. Rozsa and R. C. Tobin, Monte Carlo analysis of the electrons' motion in a segmented hollow cathode discharge, J. Phys. D, 29 (1996) 105.
10. M. Surendra and D. B. Graves, Particle simulations of radio-frequency glow discharges, IEEE Trans. Plasma Sci., 19 (1991) 144.
11. H. B. Smith, C. Charles, R. W. Boswell and H. Kuwahara, J. Appl. Phys., 82 (1997) 561.
12. M. Surendra, D. B. Graves and G. M. Jellum, Self-consistent model of a direct current glow discharge: Treatment of fast electrons, Phys. Rev. A, 41 (1990) 1112.
13. Z. Donko, Hybrid model of a rectangular hollow cathode discharge, Phys. Rev. E, 57 (1998) 7126.
14. M. A. Karolewski, Classical dynamics simulation of projectile-surface interactions, Surf. Int. Anal., 27 (1999) 114.
15. E. Dekempeneer, J. Smeets, J. Meneve, L. Eersels and R. Jacobs, Plasma processes in methane discharges during RF plasma-assisted chemical vapor deposition of a-C:H thin films, Thin Solid Films, 241 (1994) 269.

16. R. Doyle, Chemical kinetics in low pressure acetylene radio-frequency glow discharges, J. Appl. Phys., 82 (1997) 4763.
17. D. Herrebout, A. Bogaerts, M. Yan, R. Gijbels, W. Goedheer and E. Dekempeneer, One-dimensional fluid model for an rf methane plasma of interest in deposition of diamond-like carbon layers, J. Appl. Phys., 90 (2001) 570.
18. D. Herrebout, A. Bogaerts, R. Gijbels, W. J. Goedheer and A. Vanhulsel, A one-dimensional fluid model for an acetylene rf discharge: a study of the plasma chemistry, IEEE Trans. Plasma Sci., 31 (2003) 659.
19. A. Bouchoule, Technological impacts of dusty plasmas, in: Dusty Plasmas: Physics, Chemistry and Technological Impacts in Plasma Processing, A. Bouchoule (Ed.), Wiley, Chichester, (1999).
20. M. Meaudre, R. Meaudre, R. Butté and S. Vignoli, Midgap density of states in hydrogenated polymorphous silicon, J. Appl. Phys., 86 (1999) 946.
21. K. De Bleecker, A. Bogaerts, W. Goedheer and R. Gijbels, Investigation of growth mechanisms of clusters in a silane discharge with the use of a fluid model, IEEE Trans. Plasma Sci., 32 (2004) 691.
22. K. De Bleecker, A. Bogaerts, R. Gijbels and W. Goedheer, Numerical investigation of particle formation mechanisms in silane discharges, Phys. Rev. E, 69 (2004) 056409.
23. G. J. Nienhuis, W. J. Goedheer, A. E. G. Hamers, W. G. J. H. M. van Sark and J. Bezemer, A self-consistent fluid model for radio-frequency discharges in SiH_4-H_2 compared to experiments, J. Appl. Phys., 82 (1997) 2060.
24. U. V. Bhandarkar, M. T. Swihart, S. L. Girshick and U. R. Kortshagen, Modelling of silicon hydride clustering in a low-pressure silane plasma, J. Phys. D: Appl. Phys., 33 (2000) 2731.
25. U. Kortshagen and U. Bhandarkar, Modeling of particle coagulation in low pressure plasmas, Phys. Rev. E, 60 (1999) 887.
26. P. K. Shukla and A. A. Mamum, Introduction to Dusty Plasma Physics, Series in Plasma Physics, IOP Publishing, London (2002).
27. W. W. Stoffels and E. Stoffels, Physics and application of dusty low pressure plasmas, Trends in Vac. Sci. & Technol., 4 (2001) 1.
28. K. De Bleecker, A. Bogaerts and W. Goedheer, Modeling of formation and transport of nanoparticles in silane plasmas, 70 (2004) 056407.

29. M. Madani, A. Bogaerts, D. Vangeneugden and R. Gijbels, Numerical description of a Dielectric Barrier Discharge at atmospheric pressure in Nitrogen, J. Appl. Phys., submitted.
30. O. Goossens, E. Dekempeneer, D. Vangeneugden, R. Van de Leest and C. Leys, Application of atmospheric pressure dielectric barrier discharges in deposition, cleaning and activation, Surface and Coat. Technol., 142 (2001) 474.
31. Yu. B. Golubovskii, V. A. Maiorov, J. Behnke and J. F. Behnke, Modelling of the homogeneous barrier discharge in helium at atmospheric pressure, J. Phys. D: Appl. Phys., 36 (2003) 39.
32. Yu. B Golubovskii, V. A. Maiorov, J. Behnke and J. F. Behnke, Influence of interaction between charged particles and dielectric surface over a homogeneous barrier discharge in nitrogen, J. Phys. D: Appl. Phys., 35 (2002) 751.
33. C. K. Birdsall and A. B. Langdon, Plasma Physics via Computer Simulations, McGraw-Hil, New York (1985).
34. M. A. Lieberman and A. J. Lichtenberg, Principles of Plasma Discharges and Materials Processing, Wiley, New York (1994).
35. V. Georgieva, A. Bogaerts and R. Gijbels, Particle-in-cell – Monte Carlo simulation of a capacitively coupled radio-frequency Ar/CF_4 discharge: Effect of gas composition, J. Appl. Phys., 93 (2003) 2369.
36. V. Georgieva, A. Bogaerts and R. Gijbels, Numerical study of $Ar/CF_4/N_2$ discharges in single- and dual-frequency capacitively coupled plasma reactors, J. Appl. Phys., 94 (2003) 3748.
37. K. Maeshige, G. Washio, T. Yagisawa and T. Makabe, Functional design of a pulsed two-frequency capacitively coupled plasma in CF_4/Ar for SiO_2 etching, J. Appl. Phys., 91 (2002) 9494.
38. V. Georgieva, A. Bogaerts and R. Gijbels, Numerical investigation of ion-energy-distribution functions in single and dual frequency capacitively coupled plasma reactors, Phys. Rev. E, 69 (2004) 026406.
39. I. Kolev and A. Bogaerts, Numerical models of planar magnetron glow discharges, Contrib. Plasma Phys., 44 (2004) 582.
40. A. Bogaerts, Comprehensive modeling network for dc glow discharges in argon, Plasma Sources Sci. Technol., 8 (1999) 210.

41. A. Bogaerts, W. Verscharen and E. Steers, Computer simulations of crater profiles in GD-OES: Comparison with experiments and investigation of the underlying mechanisms, Spectrochim. Acta Part B, 59 (2004) 1403.
42. A. Bogaerts and R. Gijbels, Calculation of crater profiles on a flat cathode in a direct current glow discharge, and comparison with experiment, Spectrochim. Acta Part B, 52 (1997) 765.
43. V. V. Serikov, S. Kawamoto, C. F. Abrams and D. B. Graves, Atomic-scale simulation of plasma-assisted deposition of DLC films, APS Proceedings of the "22nd Symposium on Rarefied Gas Dynamics", Sydney 2000.
44. D. W. Brenner, Empirical potential for hydrocarbons for use in simulating the chemical vapor deposition of diamond films, Phys. Rev. B, 42 (1990) 9458.
45. J. Benedikt, K. G. Y. Letourneur, M. Wisse, D. C. Schram and M. C. M. van de Sanden, Diamond Rel. Mat., 11 (2002) 989.
46. E. Neyts, A. Bogaerts, R. Gijbels, J. Benedikt and M.C.M. van de Sanden, Molecular dynamics simulations for the growth of diamond-like carbon from low kinetic energy species, Diamond and Related Materials 13 (2004) 1873.
47. A.-L. Hamon, J. Verbeeck, D. Schryvers, J. Benedikt and M. C. M. van de Sanden, ELNES study of carbon K-edge spectra of plasma deposited carbon films, J. Mat. Chem., 14 (2004) 2030.